Highly Reproducible Nanolithography by Dynamic Plough of an Atomic-Force Microscope Tip and Thermal-Annealing Treatment

Xiaofeng Lu, Claudio Balocco, *Member, IEEE*, Fuhua Yang, and Aimin M. Song, *Senior Member, IEEE*

***Abstract*—An approach has been developed to use atomic-force microscope (AFM) to pattern materials at the nanoscale in a controlled manner. By introducing a thermal-annealing process above the glass-transition temperature of poly (methylmethacrylate) (PMMA), the profile of indented nanopatterns has been dramatically improved by abatement of the tip-induced debris. This eliminates the main problem of the previous AFM-based tip-ploughing lithography method, namely the debris formation during the nanoplough and trench refilling by debris. We are able to reproducibly fabricate nanopatterns down to 40 nm. Meanwhile, the AFM-tip lifetime has been increased substantially. In particular, the adhesion between the PMMA layer on the edge of trenches and the substrate is significantly improved to enable reliable pattern transfer into GaAs/AlGaAs heterostructures by wet-chemical etching. Functional nanodevices with a lateral feature size of 100 nm to an etching depth of 70 nm are demonstrated using the method.**

***Index Terms*—Atomic-force microscope (AFM), nanolithography, self-switching diodes (SSDs), 2-D electron gas.**

I. Introduction

SCANNING-probe-based nanolithography has, in recent years, gained much attention for a wide range of nanostructures and nanodevices [1]–[3]. In addition to its excellent capabilities of nondestructive imaging and spectroscopy, atomic-force microscope (AFM) has been exploited, particularly, as a convenient and flexible tool for patterning materials at the nanoscale at ambient conditions [4]–[6]. AFM-based nanolithography possesses a number of advantages over standard electron-beam lithography, such as the ease to use [7], low cost, and the possibility to perform *in situ* electrical measurements [8]. Various nanolithography approaches have been developed including mechanical modification [6], [9], local anodic oxidation [10], [11], thermal modification [12], erasable electrostatic modulation [13], and material deposition [14]. The mechanical-modification method is perhaps the most studied among these approaches that typically involves an AFM-tip ploughing, a substrate, or a polymer resist layer, either under a constant force [15]–[17] or in a dynamic-indentation mode [18]–[20]. However, the practical use of such nanolithography has so far been hampered by several problems, for instance, refilling of the trenches by debris generated during the tip ploughing, frequent-tip contamination by the debris, and poor reproducibility of the lithography.

TO overcome these drawbacks, it was recently reported that by nanoindentation of a conducting polymer poly (3-hexylthiophene-2,5-diyl) (P3HT), nanofeatures ranging from 40 nm to 2.3 μm were achieved reliably [21], [22]. The semicrystalline properties and high tensile strain of P3HT were believed to have largely eliminated issues, such as refilling of the trenches by debris, tip contamination, and short AFM-tip lifetime [3], [22]. It was also reported that AFM-tip ploughing of a thin layer of standard electron-beam lithography resist poly (methylmethacrylate) (PMMA) and subsequent metal liftoff produced metallic nanodots with a size of 70 nm and nanowires with a width of 120 nm [23]. It was not clear, however, whether pattern transfer by wet-chemical etching would be also be feasible using the tip-ploughing method due to the apparent formation of debris, and hence, possible loosening of the resist around the edges of the ploughed features.

Here, we report a novel AFM-based technique to transfer well-defined nanopatterns on a resist mask into GaAs/AlGaAs substrate by wet etching. We compared high-tensile strain P3HT films with thin amorphous PMMA films, and discovered that the latter provided much more reliable pattern transfer by wet-chemical etching. In particular, both the trench-edge definition and adhesion of the PMMA film to the substrate were significantly improved after we introduced a thermal treatment above the PMMA glass-transition temperature. The serious underetch problem was, hence, avoided and planar nanodiodes that rely on fine trench-edge definition were fabricated successfully.

II. Experiments

PMMA (molecular weight: 350 KMW) was dissolved into chlorobenzene at a concentration of about 0.41 wt%. The solution was filtered with a 0.2 μm polytetrafluoroethylene (PTFE) syringe filter to remove insoluble particles. The prepared solution was spin coated onto GaAs substrates at 3000 r/min for

Manuscript received January 27, 2010; revised May 24, 2010; accepted June 7, 2010. Date of publication June 14, 2010; date of current version January 26, 2011. This work was supported by the U.K. Technology Strategy Board through the ULTRAFINE project and a Royal Society Brain Mercer Feasibility Award. The review of this paper was arranged by Associate Editor J. Li.

X. Lu, C. Balocco, and A. M. Song are with the School of Electrical and Electronic Engineering, University of Manchester, Manchester M13 9PL, U.K. (e-mail: xiaofeng.lu@manchester.ac.uk; claudio.balocco@manchester.ac.uk; a.song@manchester.ac.uk).

F. Yang is with the State Key Laboratory for Superlattices and Microstructures, Institute of Semiconductors, Chinese Academy of Sciences, Beijing 100083, China (e-mail: fhyang@red.semi.ac.cn).

Color versions of one or more of the figures in this paper are available online at http://ieeexplore.ieee.org.

Digital Object Identifier 10.1109/TNANO.2010.2053045

1536-125X/$26.00 © 2010 IEEE

2 min. The resulted PMMA film was baked at 150 °C for 30 min. The PMMA film thickness was optimized to be around 7 nm for the suitability of both tip-indentation nanolithography and wet-chemical etching. A much thicker layer of PMMA led to much debris formation, affecting the uniformity of trenches and film adhesion to the substrate. For comparison, P3HT films were also prepared by spin coating from a solution of 0.55 wt% in trichlorobenzene and baked at 100 °C before the nanolithography. The obtained film thickness was 8 nm, approximately the same as that of the PMMA film.

After the preparation of the mask layer, nanolithography was carried out with a VEECO CP Research AFM. The AFM tips adopted in this study were Si_3N_4 one (NSC11, MikroMasch) with a radius of 20 nm and a tip angle of 40 °. Cantilevers with various spring constants were tested and a high-spring constant of 48 N/m was found to be the most suitable. For topography imagining of samples, the AFM was operated in the tapping mode rather than contact mode to avoid damaging the nanofeatures. A testing grid of indentation was made with nominal-penetration depths ranging from –0.05 to –0.3 μm. The width of indentation at a nominal depth of –0.15 μm was around 56 nm. Similar optimization experiments were carried out for P3HT films. It is worth noting that, due to the regiorandom nature of PMMA, the distance between neighboring indentations needed to be kept around 20 nm in order to achieve clean trench bottom.

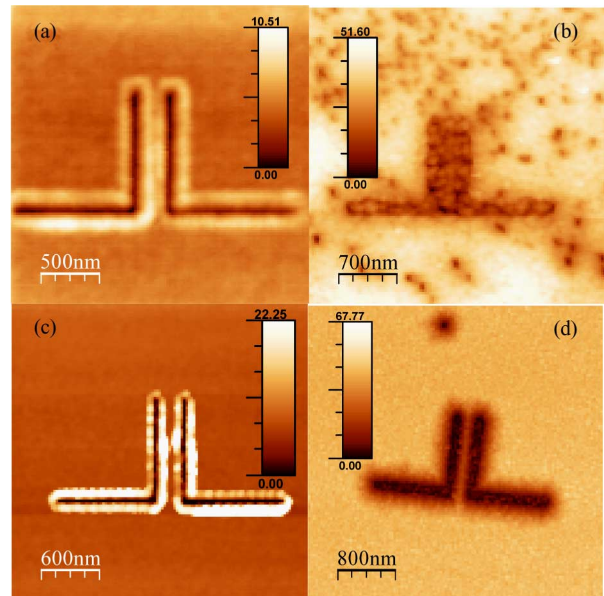

Fig. 1. Comparison of P3HT and PMMA films as etching mask. (a) AFM topography images of an SSD-like pattern in a P3HT film, showing well-defined narrow trenches fabricated by nanoindentation. (b) AFM image of the sample after wet etching into the GaAs substrate, showing serious underetch and poor protection by the thin P3HT mask after etching in a hydrogen-peroxide-based etchant. (c) Similar nanoindentation into a PMMA mask layer. (d) AFM image of etched pattern into the GaAs substrate. The definition of resulting pattern was much improved even though the underetch was still quite serious.

III. Results and Analysis

We first compared P3HT and PMMA as wet-etching resist masks. Fig. 1(a) shows narrow trenches fabricated on a 7-nm-thick P3HT layer. The pair of nanotrenches defines the active nanochannel of a planar nanodiode called self-switching device (SSD) [24]–[26]. The SSD is chosen because its electrical properties are determined by the active nanochannel, which is very sensitive to the precision and definition of nanolithography. After spin coating, the P3HT film was annealed at 100 °C in nitrogen gas. Well-defined uniform trenches were made into P3HT film by nanoindentation. The channel width between the two vertical trenches was designed to be 300 nm and it was reduced after the lithography due to the finite-trench width. Some debris was distributed rather evenly along the trench sidewalls and the debris height was around 3–4 nm. The widths of the vertical and horizontal trenches were around 65 and 67 nm, respectively. The widths of the trenches were larger than the diameter of our AFM tip (40 nm) due to the tensile strain in the P3HT film and were comparable to the results by nanoscratching previously achieved on polymer films [21], [22], [27], [28]. It is worth noting that the trench depth appeared to be less than the thickness of the P3HT film. It was most likely due to the narrowness of the trench and the surrounding debris that prevented the AFM tip from reaching the bottom.

Fig. 1(b) shows the typical AFM image after the samples were etched in $H_3PO_4/H_2O_2/H_2O$ solution (in a ratio of 3:1:50) for 90 s. The etching rate of GaAs was around 60 nm/min at room temperature. There was clearly serious under etch around the trenches, which may be due to the following two reasons. There could be poor adhesion of the P3HT layer to the substrate around the trench areas caused by the mechanical disturbance during the nanoindentation, which allowed the etching solution to diffuse through the interface between the P3HT mask layer and the substrates, and hence, caused excessive lateral etching. It can also be seen that the P3HT film was obviously attacked by the etchant. To improve the pattern transfer, we tried to anneal the P3HT film after the nanoindentation up to a temperature of 140 °C. UV-ozone treatment was also experimented to remove the debris prior to the wet etch. However, no significant improvement was observed.

Given that the tensile strain in the regioregular P3HT film might have weakened the adhesion of film to the substrate in the proximity of the indented trenches, an alternative polymer, which is regiorandom, and hence, has little strain formation might be more favorable as the etching mask. We, thus, replaced the P3HT resist with a 7-nm-thick PMMA film deposited by spin coating. Initially, in order to compare the result with that of P3HT, no postlithography treatment was applied and the sample was etched in the same hydrogen-peroxide-based etchant for 1 min at room temperature. Fig. 1(c) shows an AFM image of the nanoindentation into the PMMA film. Uniform trenches were obtained with a width of 50 nm, about the same as the diameter of the AFM tip. Debris was distributed quite evenly along the trenches. It is worth noting that a much greater amount of debris was generated than in the earlier nanoindentation of the P3HT film. This may be ascribed to the regiorandom nature of PMMA because it is expected to be easier to break a regiorandom film into small pieces than a regioregular polymer consisting of highly ordered packing of long molecules.

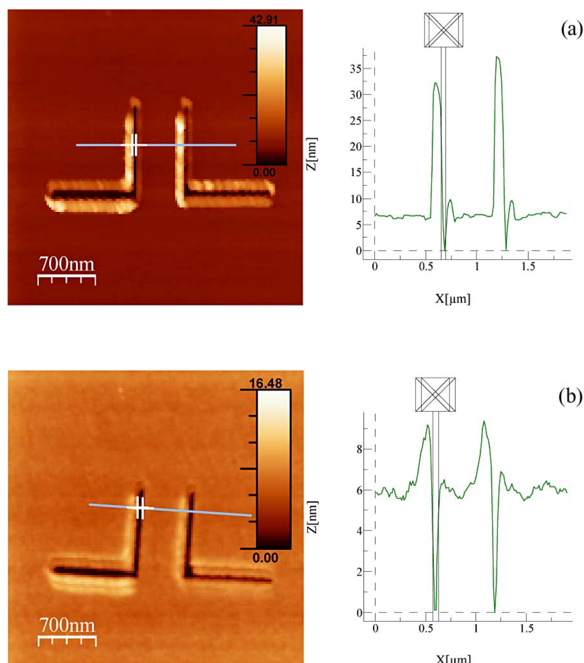

Fig. 2. AFM topography images of the same nanoploughed trenches into PMMA (a) before any annealing was carried out and (b) after annealing at 240 °C The height of the debris was dramatically reduced from about 30 to 2 nm without undermining the feature definition of nanotrenches.

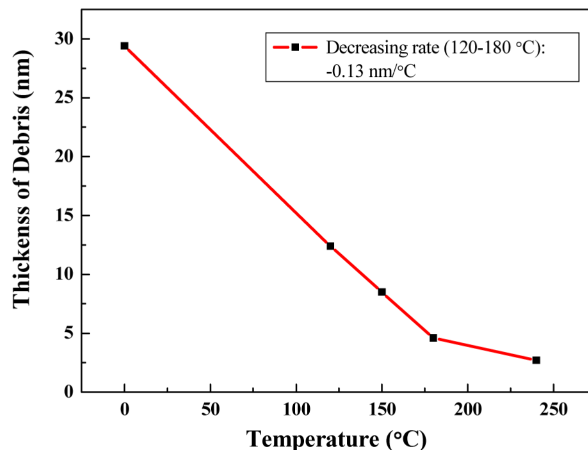

Fig. 3. Height of the debris as a function of the baking temperature after the nanolithography was carried out. A good linear relation is noted in the range from 120 to 180 °C.

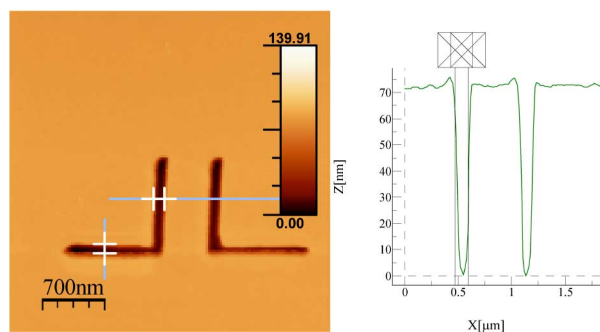

Fig. 4. AFM images of an SSD pattern after Br/HBr-based etching on a GaAs substrate. The trenches are about 100 nm wide and 70 nm deep.

The pattern transfer by wet etching was much improved than using P3HT film, as shown in Fig. 1(d), although the AFM image still reveals clear lateral etch around the trenches. Clearly, the pattern transfer in Fig. 1 would not be sufficient for practical nanoelectronic-device fabrication.

To overcome the underetch issue, we first tried to improve the adhesion between PMMA and substrate after the nanoindentation. The glass-transition temperature (T_G) of PMMA that we adopted for the experiments was 122 °C. Samples were post-baked at various temperatures 120, 150, 180, and 240 °C, after the nanoindentation was carried out into the PMMA film. The baking time was half an hour for each temperature and the sample was imaged by the AFM after each annealing to identify any change in topography. The annealing process was found to be critical to improve the trench profile once the temperature was around or above T_G. Fig. 2 shows the AFM topography images of the same nanoploughed trenches in PMMA (a) before any annealing was carried outand (b) after annealing at 240 °C. The height of the debris was dramatically reduced from about 30 to 2 nm. More importantly, the debris reduction did not obviously affect the trench depth, width, or uniformity. It indicated that PMMA debris on the edge of trenches did not tend to fill in the trenches under the high-temperature annealing. As the PMMA debris softened gradually at annealing temperatures close to or beyond T_G, the debris seemed to have spread on the neighboring PMMA film rather than collapsing into the trenches probably due to the wetting effect.

The detailed study of the reduction of debris at different annealing temperatures is shown in Fig. 3. After baking at 120 °C, the height of debris reduced from 30 to 21 nm. A rather linear relationship between the reduction of debris' height and annealing temperature was observed from 120 to 180 °C.

The dramatic improvement of the patterned profiles after the thermal treatment might also enhance the adhesion of the PMMA film, and hence, eliminate the underetch problem. Another reason for the poor etching result in Fig. 1(d) might be hydrogen peroxide attacking the PMMA etching mask. In the following experiments, we substituted the hydrogen-peroxide-based etchant with saturated bromine water and hyrobromic acid (HBr) compound. Fig. 4 shows an SSD pattern after a Br/HBr-based etching into a GaAs substrate for 45 s. Successful pattern transfer was achieved with a trench width of around 100 nm and a depth of about 70 nm in both horizontal and vertical directions. It is worth noting that the width of the trenches was much less than what would be expected for an isotropic wet etch that is 70 nm deep. This suggests that the HBr-based etchant was somehow anisotropic for GaAs that enables fine features and nanoelectronic devices to be fabricated on GaAs substrates without using reactive ion etching.

To further understand the two factors that might have improved the etching result, namely the thermal annealing after the nanoindentation and the change to HBr-based etchant, we carried out experiments under different process conditions. As illustrated in Fig. 5(a), without the postbaking treatment, the

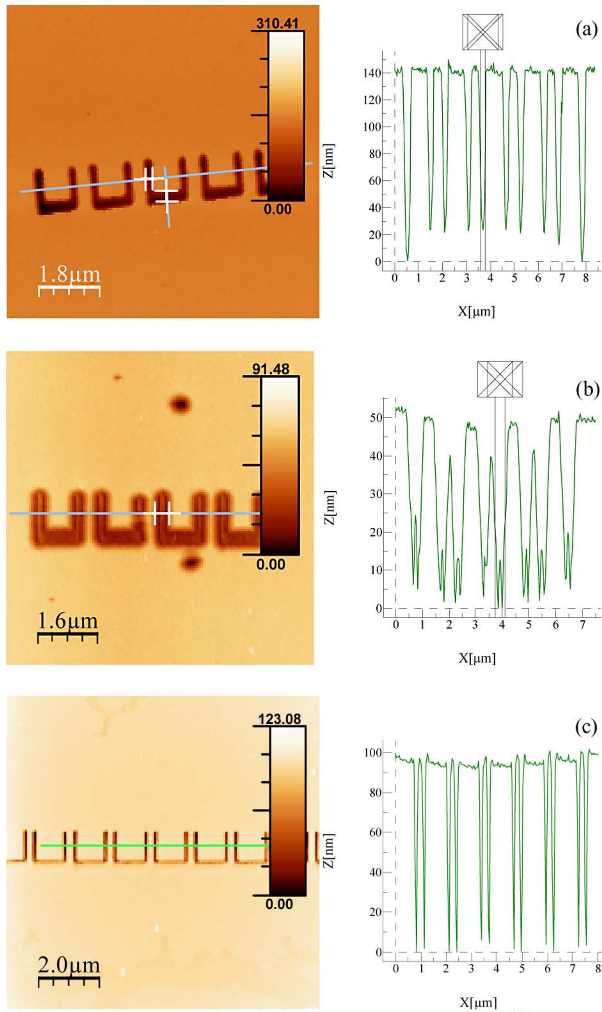

Fig. 5. AFM images of etched GaAs patterns under different process conditions. (a) No annealing was carried out after the nanoindentation and the etchant was HBr/Br based. The trench width is about 192 nm. (b) Annealing was carried out after the nanoplough and the etchant was hydrogen peroxide based. Compared to the result from the previous H_2O_2 etching processes without annealing treatment in Fig. 1(d), the trench width was reduced to around 250 nm. (c) Annealing was carried out after the nanoindentation and the etchant was HBr/Br based. The AFM image shows significant improvement of the pattern transfer, with trench width around 100 nm.

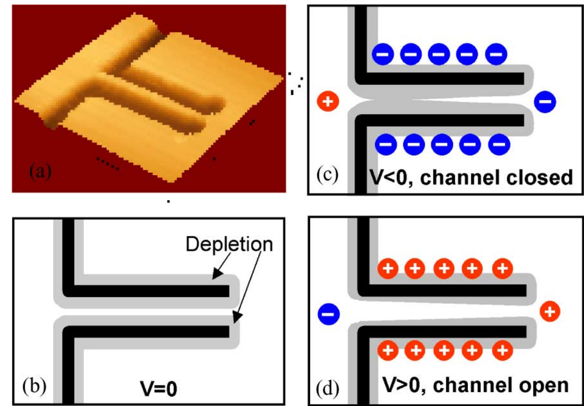

Fig. 6. Schematic diagrams showing the common geometry of an SSD planar device and the working principle. (a) AFM image of an SSD. The darker areas are the etched insulating trenches. (b) Channel is nearly depleted by the surface states on the etched boundaries. Depending on the applied voltage V, the effective width of the channel will be either reduced (c) or increased (d), giving rise to a diode-like I–V characteristic [26].

final pattern on the GaAs substrate was much larger than that in Fig. 4 (note the different scales) even with the same HBr-based etchant, indicating significant lateral etch. Despite a similar width of the trenches after the nanoindentation on PMMA (60 nm), the etched trenches in GaAs were nearly 200 nm wide. In contrast, with the same etchant but by introducing annealing after the nanoindentation, the etched trenches were only about 100 nm wide, as shown in Fig. 5(c), showing significant improvement by the introduced thermal-annealing process. Furthermore, the different impacts of the HBr- and hydrogen-peroxide-based etchants were compared. Fig. 5(b) shows the result with the thermal-annealing process and using the hydrogen-peroxide-based etchant. The underetching was clearly still serious, and the resulting trenches were about 250 nm wide. Also, the thin PMMA film could not prevent the attack of hydrogen-peroxide-based etchant to the GaAs substrate effectively. However, by comparing it to the result of the process without thermal annealing in Fig. 1(d), the quality of the pattern transfer was still enhanced substantially by the thermal annealing.

To investigate the feasibility of the aforementioned technique for nanoelectronic devices, we fabricated SSDs because they are very sensitive to fine nanotrench definition [24], [26]. Apart from being a nanomemory device, the SSD typically functions as a diode and was demonstrated to be able to detect microwave up to 110 GHz at room temperature [24] and free-space radiation up to at least 2.5 THz at temperatures below 150 K [25]. Recently, the SSD was also envisaged to function as a sub-THz emitter under a large dc bias [29]. The SSD is realized by tailoring the boundary of a narrow semiconductor channel to break its symmetry, as shown by the 3-D AFM image in Fig. 6(a). An applied voltage V not only changes the potential profile along the channel direction, but also either narrows [see Fig. 6(c)] or widens [see Fig. 6(d)] the effective channel width, depending on the sign of voltage, giving rise to a diode-like current–voltage characteristic.

However, the property of a conventional diode is mainly determined (and hence fixed) by the semiconductor materials, and the characteristics of the SSD can be tuned by varying the device geometry. For instance, the threshold voltage of SSDs can be adjusted by changing the channel width. SSD arrays with different channel widths ranging from 340 to 380 nm have been fabricated and measured. The channel length of the devices was 1 μm. From current–voltage results in Fig. 7, diode-like, asymmetric characteristics were observed in devices with 340 and 360 nm wide channels. For the SSD with a channel width of 380 nm, the characteristic became rather symmetric. This is expected because as the channel widens, it becomes more difficult to switch off the nanochannel by the negative potential on both sides of the nanotrenches, as in Fig. 6(c). To optimize the rectification ratio, we also increased the channel length from 1 to 1.5 μm. Fig. 8 shows the improved diode characteristic of a

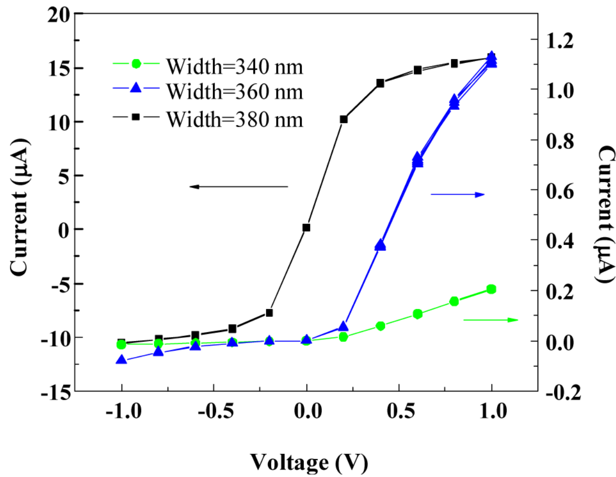

Fig. 7. Current–voltage characteristics of SSD arrays with different channel widths at room temperature. The SSD channel length was 1.0 μm.

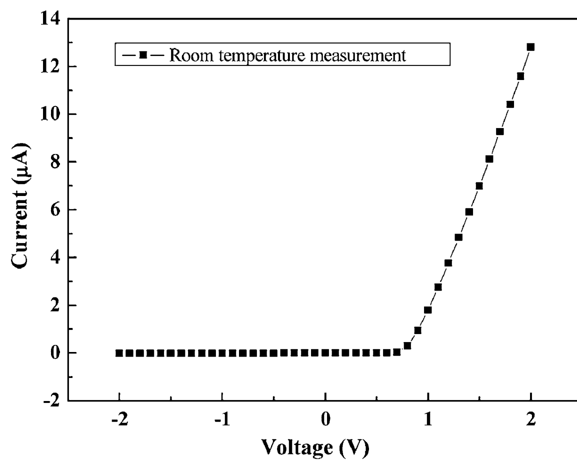

Fig. 8. Current–voltage characteristic of an SSD with a channel length of 1.5 μm and channel width of 360 nm.

device with a channel width of 360 nm. The on current reached 13 μA at $+1$ V and the off current was around nanoampere under the negative bias. This is the best rectification ratio that we have achieved so far at room temperature in our experiments.

IV. Conclusion

In summary, we have developed an alternative nanolithography method based on AFM. The method was proven to be effective for both conducting polymer and standard electron-beam lithography resist, and we could pattern trenches down to the scale of 40 nm in lateral dimensions. The major improvement was enabled by introducing a thermal-annealing treatment at suitable temperatures. This dramatically reduced the debris formed during nanoindentation, significantly enhanced the adhesion of the polymer layer after the nanoindentation, and effectively overcome the underetch problem to allow successful pattern transfer to GaAs materials. We applied the technique and demonstrated working nanodevices. Nanodiodes with a high-rectification ratio were achieved at room temperature.

References

[1] Z. Cui, *Nanofabrication*. New York: Springer Science and Business Media LLC, 2008.
[2] H. T. Soh, K. W. Guarini, and C. F. Quate, *Scanning Probe Lithography*. Boston, MA: Kluwer, 2001.
[3] A. A. Tseng, "Nanofabrication by scanning probe microscope lithography: A review," *J. Vac. Sci. Technol. B*, vol. 23, pp. 877–894, 2005.
[4] G. Binning, C. F. Quate, and Ch. Gerber, "Atomic force microscope," *Phys. Rev. Lett.*, vol. 56, pp. 930–933, 1986.
[5] X. Jin and W. N. Unertl, "Submicrometer modification of polymer surfaces with a surface force microscope," *Appl. Phys. Lett.*, vol. 61, pp. 657–659, 1992.
[6] Y. Kim and C. M. Lieber, "Machining oxide thin films with an atomic force microscope: Pattern and object formation on the nanometer scale," *Science*, vol. 257, pp. 375–377, 1992.
[7] R. Garía and R. Pérez, "Dynamic atomic force microscopy methods," *Surf. Sci. Rep.*, vol. 47, pp. 197–301, 2002.
[8] B. Irmer, M. Kehrle, H. Lorenz, and J. P. Kotthaus, "Fabrication of Ti/TiO_x tunneling barriers by tapping mode atomic force microscopy induced local oxidation," *Appl. Phys. Lett.*, vol. 71, pp. 1733–1735, 1997.
[9] M. Rolandi, I. Suez, H. Dai, and J. M. J. Fréchet, "Dendrimer monolayers as negative and positive tone resists for scanning probe lithography," *Nano Lett*, vol. 4, pp. 889–893, 2004.
[10] E. S. Snow and P. M. Campbell, "AFM fabrication of sub-10 nanometer metal-oxide devices with in Situ control of electrical properties," *Science*, vol. 270, pp. 1639–1641, 1995.
[11] A. Fuhrer, S. Luscher, T. Ihn, T. Heinzel, K. Ensslin, W. Wegscheider, and M. Bichler, "Energy spectra of quantum rings," *Nature (London)*, vol. 413, pp. 822–825, 2001.
[12] D. Wouters and U. S. Schubert, "Nanolithography and nanochemistry: Probe-related patterning techniques and chemical modification for nanometer-sized devices," *Angew. Chem. Int. Ed.*, vol. 43, pp. 2480–2495, 2004.
[13] R. Crook, A. C. Graham, C. G. Smith, I. Farrer, H. E. Beere, and D. A. Ritchie, "Erasable electrostatic lithography for quantum components," *Nature (London)*, vol. 424, pp. 751–754, 2003.
[14] T. C. Chang, C. S. Chang, H. N. Lin, and T. T. Tsong, "Creation of nanostructures on gold surfaces in nonconducting liquid," *Appl. Phys. Lett.*, vol. 67, pp. 903–905, 1995.
[15] R. Magno and B. R. Bennett, "Nanostructure patterns written in III–V semiconductors by an Atomic Force Microscope," *Appl. Phys. Lett.*, vol. 70, pp. 1855–1857, 1997.
[16] H. W. Schmacher, U. F. Kayser, U. Zeitler, and R. J. Haug, "Nanomachining of mesoscopic electronic devices using an Atomic Force Microscope," *Appl. Phys. Lett*, vol. 75, pp. 1107–1109, 1999.
[17] T. H. Fang and W. J. Chang, "Effects of AFM-based nanomachining process on aluminum surface," *J. Phys. Chem. Solids*, vol. 64, pp. 913–918, 2003.
[18] T. A. Jung, A. Moser, H. J. Hug, D. Brodbeck, R. Hofer, H. R. Hidber, and U. D. Schwarz, "The atomic force microscope used as a powerful tool for machining surfaces," *Ultramicroscopy*, vol. 42–44, pp. 1446–1451, 1992.
[19] M. Wendel, S. Kühn, H. Lorenz, and J. P. Kotthaus, "Nanolithography with an atomic force microscope for integrated fabrication of quantum electronic devices," *Appl. Phys. Lett.*, vol. 65, pp. 1775–1777, 1994.
[20] B. Cappella and H. Sturm, "Comparison between dynamic plowing lithography and nanoindentation methods," *J. Appl. Phys.*, vol. 91, pp. 506–512, 2002.
[21] A. G. Jones, C. Balocco, R. King, and A. Song, "Highly tunable, high-throughout nanolithography based on strained regioregular conducting polymer films," *Appl. Phys. Lett.*, vol. 89, pp. 013119-1–013119-3, 2006.
[22] C. Balocco, A. G. Jones, J. M. Kingsley, J. R. Chan, X. Q. Huang, and A. M. Song, "Scanningprobe microscope based on nanolithography on conducting polymer films," *Jpn. J. Appl. Phys.*, vol. 45, pp. 2095–2098, 2006.
[23] J. H. Hsu, C. Y. Lin, and H. N. Lin, "Fabrication of metallic nanostructures by atomic force microscopy nanomachining and lift-off process," *J. Vac. Sci. Technol. B.*, vol. 22, pp. 2768–2771, 2004.
[24] C. Balocco, A. M. Song, M. Åberg, A. Forchel, T. González, J. Mateos, I. Maximov, M. Missous, A. A. Rezazadeh, J. Saijets, L. Samuelson,

D. Wallin, K. Williams, L. Worschech, and H. Q. Xu, "Microwave detection at 100 GHz by nanowires with broken symmetry," *Nano Lett.*, vol. 5, pp. 1423–1427, 2005.
[25] C. Balocco and A. M. Song, "Novel semiconductor nanodevices for detection of THz signals," in *Proc. 1st IEEE Int. Conf., Nano/Micro Eng. Mol. Syst.*, 2006, pp. 1292–1296.
[26] A. M. Song, M. Missous, P. Omling, A. P. Peaker, L. Samuelson, and W. Seifert, "Unidirectional electron flow in a nanometer-scale semiconductor channel: A self-switching device," *Appl. Phys. Lett.*, vol. 83, pp. 1881–1883, 2003.
[27] B. Klehn and U. Kunze, "Nanolithography with an atomic force microscope by means of vector-scan controlled dynamic plowing," *J. Appl. Phys.*, vol. 85, pp. 3897–3903, 1999.
[28] J. H. Hsu, C. Y. Lin, and H. N. Lin, "Fabrication of metallic nanostructures by atomic force microscopy nanomachining and lift-off process," *J. Vac. Sci. Technol. B*, vol. 22, pp. 2768–2771, 2004.
[29] K. Y. Xu, X. F. Lu, A. M. Song, and G. Wang, "Teraherz harmonic generation using a planar nanoscale unipolar diode at zero bias," *Appl. Phys. Lett.*, vol. 92, pp. 163503-1–163503-3, 2008.

Authors' photographs and biographies not available at the time of publication.